

Novel Superstructure-Phase 2D Material 1T-VSe at High Pressure

Raimundas Sereika, Changyong Park, Curtis Kenney-Benson, Niall Joseph English, Sateesh Bandaru, Qiangwei Yin, Hechang Lei, Ning Chen, Cheng-Jun Sun, Steve M. Heald, Ji-Chang Ren, Jun Chang, Yang Ding, and Ho-Kwang Mao

J. Phys. Chem. Lett., **Just Accepted Manuscript** • DOI: 10.1021/acs.jpcllett.9b03247 • Publication Date (Web): 10 Dec 2019

Downloaded from pubs.acs.org on December 17, 2019

Just Accepted

“Just Accepted” manuscripts have been peer-reviewed and accepted for publication. They are posted online prior to technical editing, formatting for publication and author proofing. The American Chemical Society provides “Just Accepted” as a service to the research community to expedite the dissemination of scientific material as soon as possible after acceptance. “Just Accepted” manuscripts appear in full in PDF format accompanied by an HTML abstract. “Just Accepted” manuscripts have been fully peer reviewed, but should not be considered the official version of record. They are citable by the Digital Object Identifier (DOI®). “Just Accepted” is an optional service offered to authors. Therefore, the “Just Accepted” Web site may not include all articles that will be published in the journal. After a manuscript is technically edited and formatted, it will be removed from the “Just Accepted” Web site and published as an ASAP article. Note that technical editing may introduce minor changes to the manuscript text and/or graphics which could affect content, and all legal disclaimers and ethical guidelines that apply to the journal pertain. ACS cannot be held responsible for errors or consequences arising from the use of information contained in these “Just Accepted” manuscripts.

Novel Superstructure-Phase 2D Material 1T-VSe₂ at High Pressure

Raimundas Sereika ^{1,2}, Changyong Park ³, Curtis Kenney-Benson ³, Niall J. English ⁴, Sateesh Bandaru ⁵,
Qiangwei Yin ⁶, Hechang Lei ⁶, Ning Chen ⁷, Cheng-Jun Sun ⁸, Steve M. Heald ⁸,
Jichang Ren ⁹, Jun Chang ¹⁰, Yang Ding ¹, Ho-kwang Mao ^{1,11}

¹*Center for High Pressure Science and Technology Advanced Research, Beijing 100094, China*

²*Vytautas Magnus University, K. Donelaičio Str. 58, Kaunas 44248, Lithuania*

³*High Pressure Collaborative Access Team, X-ray Science Division, Argonne National Laboratory, Lemont, Illinois
60439, USA*

⁴*School of Chemical and Bioprocess Engineering, University College Dublin, Belfield, Dublin 4, Ireland*

⁵*College of Materials and Environmental Engineering, Institute for Advanced Magnetic Materials, Hangzhou
Dianzi University, Hangzhou 310018, China*

⁶*Department of Physics and Beijing Key Laboratory of Opto-electronic Functional Materials & Micro-nano
Devices, Renmin University of China, Beijing 100872, China*

⁷*Canadian Light Source, 44 Innovation Boulevard, Saskatoon, SK, S7N 2V3, Canada*

⁸*X-ray Science Division, Advanced Photon Source, Argonne National Laboratory, Lemont, Illinois 60439, USA*

⁹*Nano and Heterogeneous Materials Center, School of Materials Science and Engineering, Nanjing University of
Science and Technology, Nanjing 210094, People's Republic of China.*

¹⁰*College of Physics and Information Technology, Shaanxi Normal University, Xi'an 710119, P. R. China*

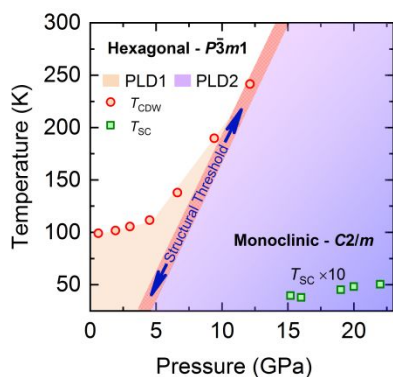
¹¹*Geophysical Laboratory, Carnegie Institution of Washington, Washington DC 20015, USA.*

*Corresponding authors: raimundas.sereika@hpstar.ac.cn; yang.ding@hpstar.ac.cn;

Abstract

A superstructure can elicit versatile new properties of materials by breaking their original geometrical symmetries. It is an important topic in the layered graphene-like two-dimensional transition-metal dichalcogenides (TMDs), but its origin remains unclear. Using diamond-anvil cell techniques, synchrotron x-ray diffraction, x-ray absorption, and the first-principles calculations, we show that the evolution from the weak Van der Waals bonding to the Heisenberg covalent bonding between layers induces an isostructural transition in quasi-two-dimensional 1T-type VSe₂ at high pressure. Furthermore, our results show that high-pressure induce a novel superstructure at 15.5 GPa, rather than suppress as it would normally, which is unexpected. It is driven by the Fermi surface nesting, enhanced by the pressure-induced distortion. The results suggest that the superstructure not only appears in the two-dimensional structure but also can emerge in the pressure-tuned three-dimensional structure with new symmetry and develop superconductivity.

TOC image.



1
2
3 Two-dimensional transition metal dichalcogenides (TMDs) exhibit rich physics, which
4 provide an ideal ‘playground’ to study novel quantum states, as well as showing promising
5 features for future advanced technological applications¹⁻³. Indeed, various modulation-
6 superstructures have been realized in TMDs^{4,5}. Periodic lattice distortion (PLD) is often
7 accompanied by charge density waves (CDW), raising the Coulombic and elastic energy as the
8 consequence and being compensated by lowering the energy of occupied electronic states.
9 According to Peierls instability, the distortion-induced kinetic energy gain is proportional to the
10 non-interacting electronic susceptibility; Fermi-surface nesting would enhance the energy gain
11 by sharply increasing the electronic susceptibility. However, in the TMDs with a superlattice,
12 Density-Functional Theory (DFT) calculations have claimed that singularities in the
13 susceptibility are not such a prerequisite towards realizing superstructures, while angle-resolved
14 photoemission spectroscopy also found no sharp Fermi-surface nesting. Therefore, the origins of
15 the TMD superstructures, which are commonly attributed to either electron-phonon coupling or
16 Fermi-surface nesting, warrant further elucidation and clarification. Moreover, many studies
17 have contributed to enhancing our understanding of low-temperature physics of TMDs. However,
18 phenomena related to the superstructure transitions under high pressure have yet to be explored
19 comprehensively in these 2-D systems, although recent progress in this regard has been
20 somewhat encouraging⁶⁻¹⁰.

21
22
23
24
25
26
27
28
29
30
31
32
33
34
35
36
37
38
39
40
41
42
43
44
45 Vanadium diselenide (VSe₂), in its 1*T* polytype, has a super-lattice incommensurate with
46 the primitive lattice (*i.e.*, a case of periodic lattice distortion coupled to charge-density waves,
47 PLD-CDW), which is distinct from those in the other 1*T* or 2*H* TMDs because of its CDW
48 transition temperature increasing with pressure¹¹. The PLD-CDW super-lattice in VSe₂ is
49 characterized by a commensurate $4\mathbf{a}_0 \times 4\mathbf{a}_0$ super-lattice forming in the layer plane and an
50
51
52
53
54
55
56
57
58
59
60

1
2
3 incommensurate $\sim 3c_0$ super-lattice forming perpendicularly to the layers at ~ 80 K¹². The strong
4
5 covalent bonding and small overlap of electron-wave functions inside the metallic layers result in
6
7 quasi-two-dimensionality and the high anisotropy of physical properties at ambient conditions.
8
9
10 The layers are linked with weak van der Waals forces allowing various creative materials-design
11
12 possibilities, such as the intercalation of foreign atoms and molecules¹³, exfoliation of the sample
13
14 to the desired number of layers^{14,15}, as well as applications in electronic devices^{16,17}. Intriguingly,
15
16 recent studies of VSe₂ revealed dramatic changes in the CDW and new physical properties such
17
18 as a pseudo-gap, Fermi arc, and emergent superconductivity¹⁸⁻²¹; naturally, this motivates us to
19
20 investigate the behavior of this material under high pressure.
21
22

23
24 In this study, by using the diamond-anvil cell (DAC)²², synchrotron x-ray diffraction
25
26 (XRD), x-ray absorption (XAS), as well as the first-principles calculations, we discovered an
27
28 isostructural transition at around 6.5 GPa and a novel superstructure PLD phase at ~ 15 GPa
29
30 occurring in 1T-VSe₂. According to the XRD results and first-principles calculations, the high-
31
32 pressure superstructure phase is associated with both the distortion of the structure and Fermi-
33
34 surface nesting. The isostructural transitions in TMDs are commonly observed under high
35
36 pressure^{23,24}. However, it is unusual that application of high pressure induces a new symmetrized
37
38 phase with a super-lattice, when pressure commonly suppresses such superstructures.
39
40

41
42 To investigate the superstructure and the phase transition at high pressure, we applied
43
44 single-crystal zone-axis x-ray diffraction. This technique has been intensively used in
45
46 transmission-electron microscopy (TEM) and has recently also been introduced into the field of
47
48 synchrotron single-crystal x-ray diffraction^{25,26}. The unique advantage of this technique lies in its
49
50 ability to study very weak satellites in a tiny portion of the reciprocal space in the low scattering
51
52 angle region. We measured the diffraction patterns along the [001] zone axis of 1T-VSe₂ at a
53
54
55
56
57
58
59
60

1
2
3 variable pressure-temperature range (with details given in the Supporting Information). During
4
5 compression, a super-lattice with commensurate peaks appeared along the original a -axis at ~ 15
6
7 GPa, 298 K (see Fig. 1). When lowering the temperature, we noticed that the transition
8
9 temperature for the super-lattice decreased with increasing pressure within the experimental P - T
10
11 range. However, single-crystal zone-axis x-ray diffraction is limited by its small reception of the
12
13 reciprocal space, incomplete peak profiles, and less accurate lattice parameters^{25,26}. Therefore,
14
15 we also performed powder x-ray diffraction experiments to provide additional information on the
16
17 larger reciprocal space in the high scattering angle region, more accurate lattice parameters, and
18
19 better peak profiles.
20
21
22
23

24 In Figure 2a, we show the phase transitions observed by the synchrotron x-ray diffraction
25
26 for $1T$ -VSe₂ powders. The structural transition occurs at 15.5 GPa, evidenced by a significant
27
28 broadening of peak (01 $\bar{1}$) and the appearance of new peaks in the diffraction patterns (Fig. 2b).
29
30 In the meantime, the single-crystal zone-axis diffraction also shows some satellites appearing at
31
32 (1/3, 0, 0) at nearly the same pressure value, thereby suggesting a $3\times 1\times 1$ commensurate
33
34 superstructure forming in a new symmetrized phase. By indexing the powder diffraction patterns
35
36 of the new phase, we determined the sample transforms from trigonal $P\bar{3}m1$ into a monoclinic
37
38 phase. Furthermore, powder x-ray diffraction measurements revealed an isostructural transition
39
40 occurring around 6.7 GPa that is signaled by a sudden change in the pressure-dependent c/a ratio
41
42 (see in Figs. 3b). A faster nonlinear decrease of c/a ratio with the pressure, before the transition,
43
44 indicates that the cell parameter c is more compressible than a in this pressure range. Such
45
46 anisotropic compressibility is attributed to the difference between the weaker van der Waals
47
48 interlayer bonding and the stronger intralayer covalent bonding. Then, a slower, roughly linear
49
50 decrease of c/a , observed after the transition, suggests that the cell parameters a and c have
51
52
53
54
55
56
57
58
59
60

1
2
3 nearly equal compressibility. The interlayer space hedged by Se atoms shrinks continuously
4 under pressure, where the shortest distance between Se atoms decreases before finally resulting
5 in bond formation at the structural transition (Fig. 3d).
6
7
8
9

10 Determining a structure model directly from the powder x-ray diffraction patterns is
11 challenging even at ambient conditions and becomes even more so in high-pressure
12 environments where the background significantly complicates the intensity and profiles of the
13 peaks. To tackle this problem, we created a $3\times 3\times 3$ supercell based on the structure at the ambient
14 conditions and searched for a possible high-pressure structural model using evolutionary
15 metadynamics²⁷ implemented in the USPEX software²⁸. Then, the resultant structure models
16 were optimized using the Vienna *ab-initio* simulation package VASP²⁹ by minimizing the total
17 energy and force on the atom with a converged criterion below 10^{-4} eV/Å (with more details
18 given in Supporting Information). Three structure models were finally determined from the
19 calculations, which all have super-lattices with the same symmetry of $C2/m$ (No. 12) but in
20 different unit cell shapes: (1) for #1 model, $a = 11.7824$ Å, $b = 3.0502$ Å, $c = 12.0426$ Å, $\beta =$
21 142.8996° , $V = 261.07$ Å³; (2) for #2 model, $a = 11.7824$ Å, $b = 3.0502$ Å, $c = 15.7368$ Å, $\beta =$
22 152.5089° , $V = 261.07$ Å³; (3) for #3 model, $a = 15.9810$ Å, $b = 3.0744$ Å, $c = 5.3157$ Å, $\beta =$
23 89.9929° , $V = 261.17$ Å³. These three models have similar total energies for their ground states
24 at high pressure. To benchmark the results from the prediction, we simulated the diffraction
25 patterns to compare them with the experimental patterns (with more details in Supporting
26 Information). The generated powder XRD patterns from the three models all match well with
27 that the experimental data (see Fig. 2c), but only the #3 structure model reproduces the
28 experimental single-crystal zone-axis diffraction pattern (see inset of Fig. 2d and Fig. S3), while
29 the other two models fail. In the zone-axis diffraction pattern of the high-pressure phase, the
30
31
32
33
34
35
36
37
38
39
40
41
42
43
44
45
46
47
48
49
50
51
52
53
54
55
56
57
58
59
60

1
2
3 orientation of the $3\times 1\times 1$ supercell relative to the lattice of the original ambient phase is $a_{super}||$
4
5 $3a_{amb}; b_{super}||[110]_{amb}; c_{super}||c_{amb}$.

6
7
8 The bulk modulus of the sample is obtained by fitting the pressure-volume data to the
9
10 third-order Birch-Murnaghan equation of state (Fig. 3a). For higher pressures, the increase of the
11
12 bulk modulus with pressure indicates the hardening of the sample. The optimized structural
13
14 model also reveals the origin of the $3\times 1\times 1$ high-pressure superstructure (Figure 3c). For instance,
15
16 the high-pressure superstructure shows a close similarity to the structure of the ambient phase,
17
18 which can be derived from the ambient phase structure by displacing two V atoms (labeled as V2
19
20 in Figure 3c) out of the a - b plane with a small distance ($\sim 0.0026\%$ along c -axis). Moreover, the
21
22 octahedral site formed by one V2 atom and its surrounding 6 Se atoms is more distorted than
23
24 other V-centered octahedral sites. It is the displacement of the V2 atom that breaks the original
25
26 translation symmetry and results in a tripled periodicity along the a -axis of the initial phase, as
27
28 well as a new symmetrized structure. Such a superstructure manifests a structural distortion (in
29
30 which V atoms deviate from their original positions and form a distorted octahedral site) which
31
32 originates from the bonds forming between layers at high pressure.
33
34
35
36
37

38 In Figure 4, we plot the temperature-pressure dependent structural change from trigonal $P\bar{3}$
39
40 $m1$ to monoclinic $C2/m$ together with the CDW and superconductivity results from Ref. 21.
41
42 Here, our data shows consistency with the CDW evolution, which is interrupted by the new
43
44 structure at 12 GPa, 240 K. The fracture in the CDW onset curve at 4.5 GPa could be the same
45
46 isostructural transition that we observed using powder XRD at 6.7 GPa (room temperature). The
47
48 superconductivity appears after the CDW collapse in the superstructure at 15 GPa, 4 K.
49
50
51

52 To investigate how the transitions affect the electronic structures of the sample, we
53
54 performed additional high-pressure XAS measurements at the Se K -edge (~ 12.66 keV) to
55
56
57
58
59
60

1
2
3 explore the unoccupied p -bands of Se at high pressure. The room temperature X-ray absorption
4 near edge structure (XANES) (demonstrated in Fig. 5) show significant pressure dependency
5
6 changes in a data region A (~ 12.70 keV). It is characterized by two trends T1 and T2,
7
8 representing the peak-energy position shift and the peak-intensity decrease with broadening
9
10 during sample compression, respectively. The pressure dependency changes in energy region A
11
12 (Fig. 5 and Figs. S5-S7) are approximately standard for the unoccupied DOS of Se p bands,
13
14 which broaden significantly after the isostructural transition. The broadening of the occupied $4p$
15
16 bands is associated with the bonding formation (more delocalization) between the Se atoms in
17
18 two different layers during the isostructural transition around 6.7 GPa. The isostructural
19
20 transition eventually leads to the van der Waals force between layers evolving into the
21
22 Heisenberg exchange interaction under pressure. In contrast, the transition at ~ 15.5 GPa causes
23
24 no sizable changes in the peak A, implying that the second transition has no dramatic effects on
25
26 the Se p bands. This is consistent with the XRD result that the superstructure is mainly
27
28 associated with the tiny displacement of V atoms. However, according to our first-principles
29
30 calculations, it is noticeable that for the ambient phase in symmetry $P\bar{3}m1$, the density of states
31
32 (DOS) of vanadium at E_F are dominant, while for the high-pressure phase in symmetry $C2/m$,
33
34 the DOS of selenium is increased substantially – ‘overwhelming’ those of vanadium (Fig. S8).
35
36 The change in the orbital components at Fermi level should be responsible for the continuous
37
38 evolution of XANES feature in the energy region A observed in the XAS of the Se K -edge.
39
40 Intriguingly, the exfoliation of other TMDs does not change peak A in a similar fashion in x-ray
41
42 absorption’s near-edge structure during the structure transitions³⁰.
43
44
45
46
47
48
49
50

51 Furthermore, in low-dimensional systems, the formation of a super-lattice is usually
52
53 associated with either structural distortion (*e.g.*, electron-phonon coupling) or Fermi-surface
54
55
56
57
58
59
60

1
2
3 nesting. At ambient conditions, vanadium diselenide possesses a type II CDW with structural
4 distortion (electron-phonon coupling)^{18,31}. However, the high-pressure magneto-resistance and
5 Hall measurements suggest successive electronic structural changes with Fermi-surface topology
6 at 6 GPa and 12 GPa, which match relatively well our defined isostructural and super-lattice-type
7 transitions, respectively. In addition, our calculations based on the high-pressure structure model
8 #3 (displayed in Fig. 3c) also reveal a Fermi-surface nesting vector existing in the superstructure
9 (Fig. S9). Considering that the structural distortion and the Fermi-surface nesting vector both
10 exist in the new superstructure phase, the origin of the superstructure may be a Fermi-surface
11 nesting driven periodic lattice distortion.
12
13
14
15
16
17
18
19
20
21
22
23

24 In conclusion, our experimental XRD and XAS room-temperature high-pressure studies
25 revealed that $1T\text{-VSe}_2$ undergoes two transitions: an isostructural one at 6.7 GPa and a structural
26 one at 15.5 GPa. The first transition was associated with layer sliding and anisotropic-isotropic-
27 contraction change between lattice parameters. At this transition, the weak van der Waals bonds
28 between layers eventually transfers into the strong covalent bonds under pressure. The second
29 transition induces a $3\times 1\times 1$ superstructure, which has lower symmetry than $P\bar{3}m1$. Using
30 theoretical structure-prediction tools, we found that the new phase should be monoclinic $C2/m$
31 where the superstructure is associated with V atoms displacement. The first-principles
32 calculations suggest that Fermi surface nesting is involved in the super-lattice formation because
33 the high-pressure phase contains wave vectors of the electrons corresponding to the Fermi
34 energy. This exciting (and, to our knowledge, unique) discovery proves that superstructure not
35 only emerges in two-dimensional structures, but paves the way for pressure tuning of three-
36 dimensional structures to manipulate and engineer novel symmetry for disparate real-world
37 applications, such as developing superconductivity.
38
39
40
41
42
43
44
45
46
47
48
49
50
51
52
53
54
55
56
57
58
59
60

Supporting Information

The Supporting Information containing detailed calculations, further numerical results, and further analysis of experimental data is available at [the link will be given by the journal].

Acknowledgements

Portions of this work were performed at HPCAT (Sector 16), and XSD (Sector 20) of Advanced Photon Source (APS), Argonne National Laboratory. HPCAT operations are supported by DOE-NNSA's Office of Experimental Sciences. XSD operations are supported by the U.S. Department of Energy (DOE) and the Canadian Light Source (CLS). The APS is a DOE Office of Science User Facility operated for the DOE Office of Science by Argonne National Laboratory under Contract No. DE-AC02-06CH11357. Y.D and H.-k.M. acknowledges the support from National Key Research and Development Program of China 2018YFA0305703, Science Challenge Project, No TZ2016001 and The National Natural Science Foundation of China (NSFC): U1930401, 11874075. H.C.L. acknowledges the support from the National Key Research and Development Program of China (Grants No. 2016YFA0300504), the NSFC (No. 11574394, 11774423, 11822412), the Fundamental Research Funds for the Central Universities, and the Research Funds of Renmin University of China (RUC) (15XNLQ07, 18XNLG14, 19XNLG17). S.B. and N.J.E. thank Science Foundation Ireland for support under the SFI-NSFC bilateral programme (SFI 17/NSFC/5229).

References

- (1) Sipos, B.; Kusmartseva, A. F.; Akrap, A.; Berger, H.; Forró, L.; Tutiš, E. From Mott state to superconductivity in $1T\text{-TaS}_2$. *Nat. Mater.* **2008**, *7*, 960–965.
- (2) Kusmartseva, A. F.; Sipos, B.; Berger, H.; Forró, L.; Tutiš, E. Pressure Induced Superconductivity in Pristine $1T\text{-TiSe}_2$. *Phys. Rev. Lett.* **2009**, *103*, 236401.
- (3) Nayak, A. P.; Bhattacharyya, S.; Zhu, J.; Liu, J.; Wu, X.; Pandey, T.; Jin, C.; Singh, A. K.;

- Akinwande, D.; Lin, J.-F. Pressure-induced semiconducting to metallic transition in multilayered molybdenum disulphide. *Nat. Commun.* **2014**, *5*, 3731.
- (4) Rossnagel, K. On the origin of charge-density waves in select layered transition-metal dichalcogenides. *J. Phys.: Condens. Matter* **2011**, *23*, 213001.
- (5) Weber, F.; Rosenkranz, S.; Castellán, J.-P.; Osborn, R.; Hott, R.; Heid, R.; Bohnen, K.-P.; Egami, T.; Said, A. H.; Reznik, D. Extended Phonon Collapse and the Origin of the Charge-Density Wave in $2H\text{-NbSe}_2$. *Phys. Rev. Lett.* **2011**, *107*, 107403.
- (6) Zhao, Z.; Zhang, H.; Yuan, H.; Wang, S.; Lin, Y.; Zeng, Q.; Xu, G.; Liu, Z.; Solanki, G. K.; Patel, K. D.; Cui, Y.; Hwang, H. Y.; Mao, W. L. Pressure induced metallization with absence of structural transition in layered molybdenum diselenide. *Nat. Commun.* **2015**, *6*, 7312.
- (7) Ma, Y.; Dai, Y.; Guo, M.; Niu, C.; Zhu, Y.; Huang, B. Evidence of the Existence of Magnetism in Pristine VX_2 Monolayers ($X = \text{S}, \text{Se}$) and Their Strain-Induced Tunable Magnetic Properties. *ACS Nano* **2012**, *6*, 1695–1701.
- (8) Ying, J.; Paudyal, H.; Heil, C.; Chen, X.-J.; Struzhkin, V. V.; Margine, E. R. Unusual Pressure-Induced Periodic Lattice Distortion in SnSe_2 . *Phys. Rev. Lett.* **2018**, *121*, 027003.
- (9) Wang, B.; Liu, Y.; Ishigaki, K.; Matsubayashi, K.; Cheng, J.; Lu, W.; Sun, Y.; Uwatoko, Y. Pressure-induced bulk superconductivity in a layered transition-metal dichalcogenide $1T\text{-tantalum selenium}$. *Phys. Rev. B* **2017**, *95*, 220501(R).
- (10) Dutta, U.; Malavi, P. S.; Sahoo, S.; Joseph, B.; Karmakar, S. Pressure-induced superconductivity in semimetallic $1T\text{-TiTe}_2$ and its persistence upon decompression. *Phys. Rev. B* **2018**, *97*, 060503(R).
- (11) Friend, R. H.; Jerome, D.; Schleich, D. M.; Molinie, P. Pressure Enhancement of Charge Density Wave Formation in VSe_2 ; The Role of Coulomb Correlations. *Solid State Commun.* **1978**, *27*, 169–173. Original paper: Chan, S.-K.; Heine, V. Spin density wave and soft phonon mode from nesting Fermi surfaces. *J. Phys. F* **1973**, *3*, 795.
- (12) Giambattista, B.; Slough, C. G.; McNairy, W. W.; Coleman, R. V. Scanning tunneling microscopy of atoms and charge-density waves in $1T\text{-TaS}_2$, $1T\text{-TaSe}_2$, and $1T\text{-VSe}_2$. *Phys. Rev. B* **1990**, *41*, 10082.
- (13) Ekvall, I.; Brauer, H. E.; Wahlström, E.; Olin, H. Locally modified charge-density waves in Na intercalated VSe_2 studied by scanning tunneling microscopy and spectroscopy. *Phys. Rev. B* **1999**, *59*, 7751.
- (14) Wang, Y.; Sofer, Z.; Luxa, J.; Pumera, M. Lithium Exfoliated Vanadium Dichalcogenides (VS_2 , VSe_2 , VTe_2) Exhibit Dramatically Different Properties from Their Bulk Counterparts. *Adv. Mater. Interfaces* **2016**, *3*, 1600433.
- (15) Pásztor, Á.; Scarfato, A.; Barreteau, C.; Giannini, E.; Renner, C. Dimensional crossover of the charge density wave transition in thin exfoliated VSe_2 . *2D Mater.* **2017**, *4*, 041005.
- (16) Zhang, Z.; Niu, J.; Yang, P.; Gong, Y.; Ji, Q.; Shi, J.; Fang, Q.; Jiang, S.; Li, H.; Zhou, X.; Gu, L.; Wu, X.; Zhang, Y. Van der Waals Epitaxial Growth of 2D Metallic Vanadium Diselenide Single Crystals and their Extra-High Electrical Conductivity. *Adv. Mater.* **2017**, *29*, 1702359.
- (17) Wang, C.; Wu, X.; Ma, Y.; Mu, G.; Li, Y.; Luo, C.; Xu, H.; Zhang, Y.; Yang, J.; Tang, X.; Zhang, J.; Bao, W.; Duan, C. Metallic few-layered VSe_2 nanosheets: high twodimensional conductivity for flexible in-plane solidstate supercapacitors. *J. Mater. Chem. A* **2018**, *6*, 8299–8306.
- (18) Chen, P.; Pai, W. W.; Chan, Y.-H.; Madhavan, V.; Chou, M. Y.; Mo, S.-K.; Fedorov, A.-

- V.; Chiang, T.-C. Unique Gap Structure and Symmetry of the Charge Density Wave in Single-Layer VSe₂. *Phys. Rev. Lett.* **2018**, *121*, 196402.
- (19) Feng, J.; Biswas, D.; Rajan, A.; Watson, M. D.; Mazzola, F.; Clark, O. J.; Underwood, K.; Markovi, I.; McLaren, M.; Hunter, A.; Burn, D. M.; Duffy, L.; Barua, S.; Balakrishnan, G.; Bertran, F.; Fevre, P. L.; Kim, T.; van der Laan, G.; Hesjedal, T.; Wahl, P.; King, P. D. C. Electronic Structure and Enhanced Charge-Density Wave Order of Monolayer VSe₂. *Nano Lett.* **2018**, *18*, 4493–4499.
- (20) Umemoto, Y.; Sugawara, K.; Nakata, Y.; Takahashi, T.; Sato, T. Pseudogap, Fermi arc, and Peierls-insulating phase induced by 3D–2D crossover in monolayer VSe₂. *Nano Res.* **2019**, *12*, 165–169.
- (21) Sahoo, S.; Dutta, U.; Harnagea, L.; Sood, A. K.; Karmakar, S. Pressure-induced suppression of charge density wave and emergence of Superconductivity in 1T-VSe₂. arXiv:1908.11678.
- (22) Mao, H.-K.; Chen, X.; Ding, Y.; Li, B.; Wang, L. Solids, liquids, and gases under high pressure. *Rev. Mod. Phys.* **2018**, *90*, 015007.
- (23) Wang, X.; Chen, X.; Zhou, Y.; Park, C.; An, C.; Zhou, Y.; Zhang, R.; Gu, C.; Yang, W.; Yang, Z. Pressure-induced iso-structural phase transition and metallization in WSe₂. *Sci. Rep.* **2017**, *7*, 46694.
- (24) Rajaji, V.; Dutta, U.; Sreeparvathy, P. C.; Sarma, S. C.; Sorb, Y. A.; Joseph, B.; Sahoo, S.; Peter, S. C.; Kanchana, V.; Narayana, C. Structural, vibrational, and electrical properties of 1T-TiTe₂ under hydrostatic pressure: Experiments and theory. *Phys. Rev. B* **2018**, *97*, 085107.
- (25) Ding, Y.; Liu, H.; Xu, J.; Prewitt, C. T.; Hemley, R. J.; Mao, H.-K. Zone-axis diffraction study of pressure-induced inhomogeneity in single-crystal Fe_{1-x}O. *Appl. Phys. Lett.* **2005**, *87*, 041912.
- (26) Ding, Y.; Liu, H.; Somayazulu, M.; Meng, Y.; Xu, J.; Prewitt, C. T.; Hemley, R. J.; Mao, H.-K. Zone-axis x-ray diffraction of single-crystal Fe_{1-x}O under pressure. *Phys. Rev. B* **2005**, *72*, 174109.
- (27) Zhu, Q.; Oganov, A. R.; Lyakhov, A. O. Evolutionary metadynamics: a novel method to predict crystal structures. *CrystEngComm* **2012**, *14*, 3596.
- (28) Lyakhov, A. O.; Oganov, A. R.; Stokes, H. T.; Zhu, Q. New developments in evolutionary structure prediction algorithm USPEX. *Comp. Phys. Comm.* **2013**, *184*, 1172–1182.
- (29) Kresse, G.; Furthmüller, J. Efficient iterative schemes for *ab initio* total-energy calculations using a plane-wave basis set. *Phys. Rev. B* **1996**, *54*, 11169–11186.
- (30) Gordon, R. A.; Yang, D.; Crozier, E. D.; Jiang, D. T.; Frindt, R. F. Structures of exfoliated single layers of WS₂, MoS₂, and MoSe₂ in aqueous suspension. *Phys. Rev. B* **2002**, *65*, 125407.
- (31) Zhu, X.; Cao, Y.; Zhang, J.; Plummer, E. W.; Guo, J. Classification of charge density waves based on their nature. *Proc. Natl. Acad. Sci. USA* **2015**, *112*, 2367–2371.

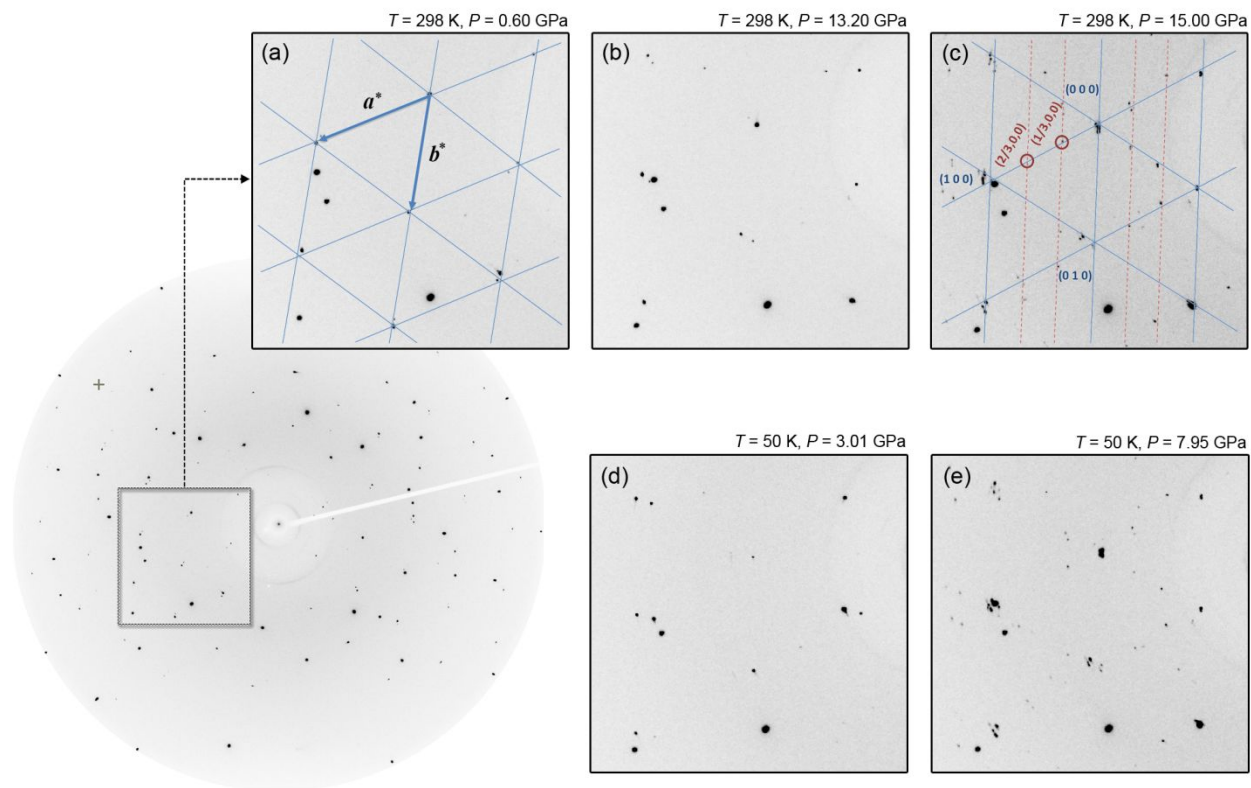


Figure 1. Diffraction images at different temperature-pressure conditions indicating a phase transition with superlattice reflections in $1T$ -VSe₂. New peaks appear on the a -axis, as marked by dashed red lines, prior to the ambient lattice, which is denoted by the solid blue lines (unmarked images given in the Supporting Information). Here, a^* and b^* are the trigonal lattice parameters in the reciprocal space before the transition. Measurement data also revealed crystal twinning, which is evident by the presence of the additional symmetrical reflections. Note: this XRD measurement is not intended to show the CDW. Images may contain peaks from diamonds, Ne gas, and the cryostat window.

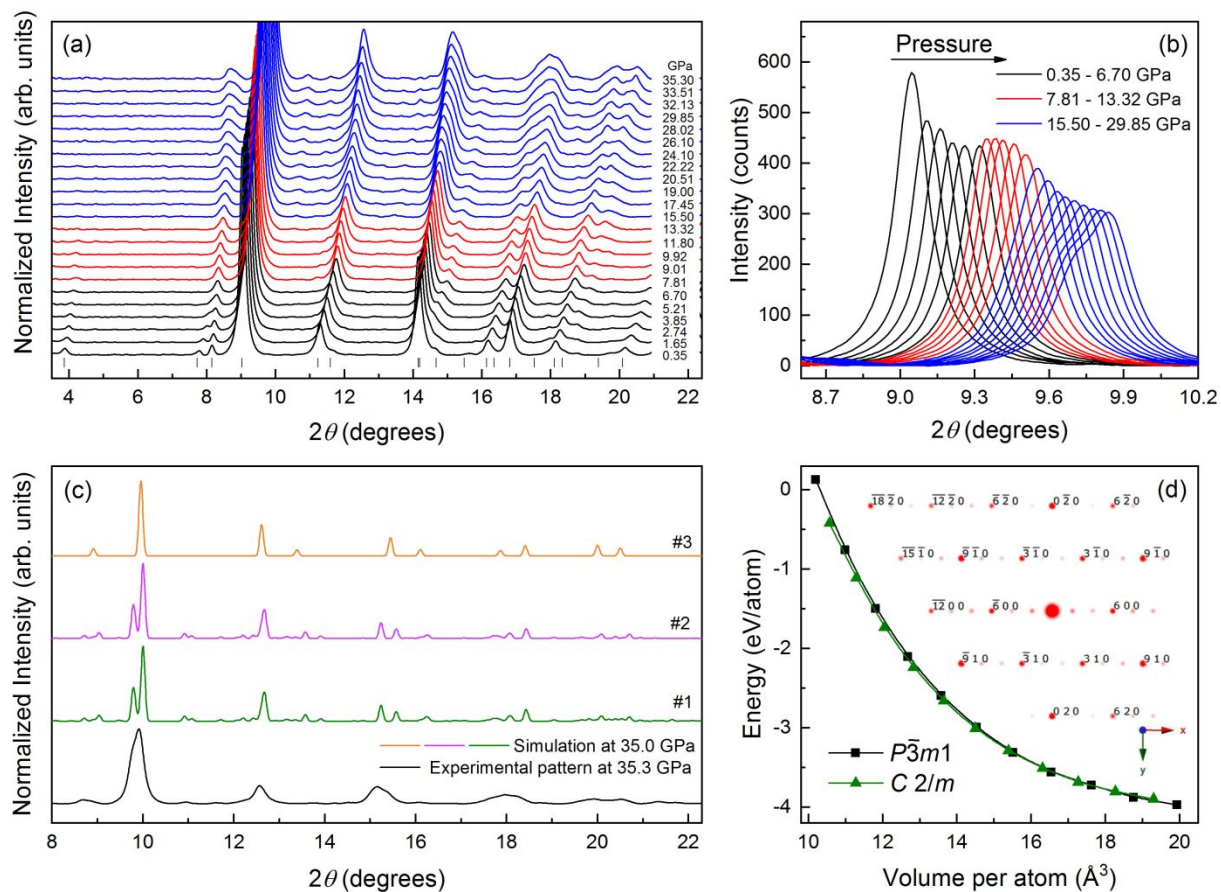


Figure 2. Synchrotron x-ray diffraction data for 1T-VSe₂ powders compared with the simulated results. The X-ray wavelength is 0.4133 Å. (a) The evolution of diffraction patterns over sample compression at room temperature. The positions of the initial $P\bar{3}m1$ Bragg reflections are marked by vertical bars. (b) The profile of the $(01\bar{1})$ peak at different ranges of pressure indicating its continuous intensity reduction and splitting. (c) The simulated XRD patterns for the high-pressure phase compared with experimental data at the same pressure. (d) Energies as a function of volume/atom calculated using GGA+ U_{eff} . The inset shows a portion of the simulated reciprocal lattice of the monoclinic phase #3 (full image is given in the Supporting Information).

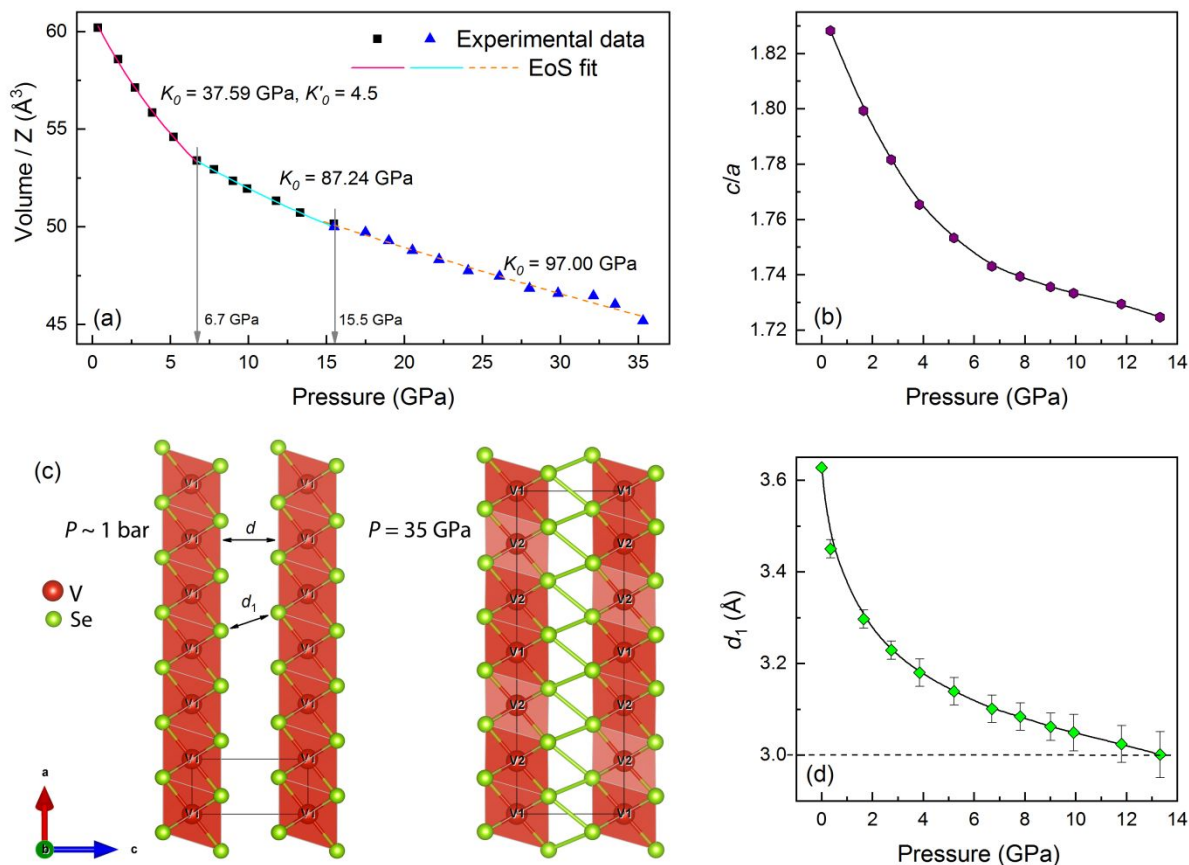


Figure 3. Changes of the unit cell in the 1T-VSe₂ at different pressures. (a) Volumes per formula unit as a function of pressure for $P\bar{3}m1$ (black squares) and $C2/m$ (blue triangles) phases. The solid and dashed lines are the calculated third-order Birch–Murnaghan equation of state (EoS) fit to the experimental data. (b) Pressure dependence of the axial ratio c/a before the structural transition. (c) Crystal structure view of the a - c plane in the ambient $P\bar{3}m1$ phase and simulated high-pressure $C2/m$ phase (35 GPa pressure). Thick solid lines indicate the unit cell. 2-D layers consist of vanadium-centered polyhedrons stacked along the c -axis. (d) Pressure dependence of the shortest Se-Se distance d_1 in the interlayer space.

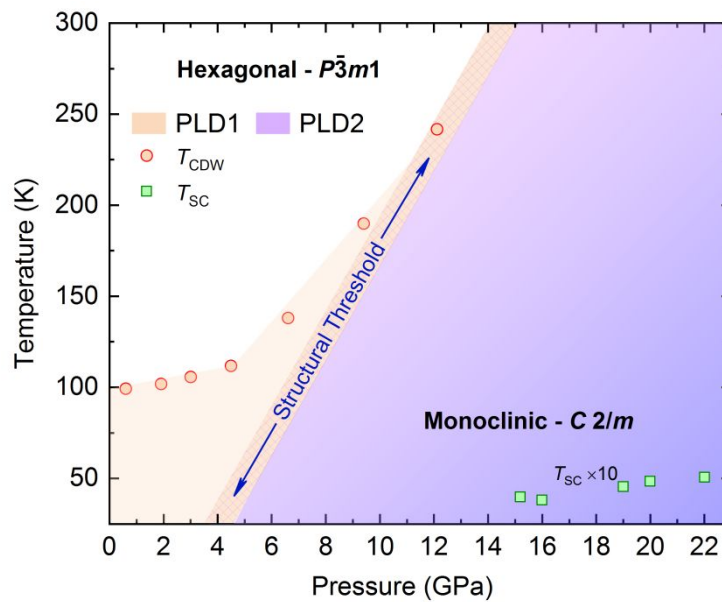


Figure 4. Structural changes in the 1T-VSe₂ at different temperatures and pressures. Periodic lattice distortions in the pressure range from 0 to 23 GPa and a temperature range from 25 to 300 K for 1T-VSe₂. The structural threshold is drawn from our low temperature single-crystal zone-axis XRD data. The data points for T_{CDW} and T_{SC} were taken from Ref. 21.

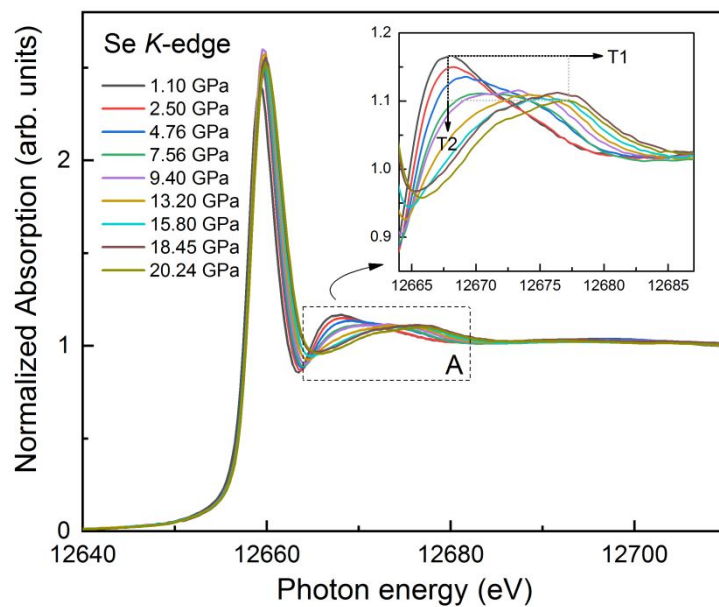


Figure 5. Normalized absorption spectra of 1T-VSe₂ at the Se K-edge as a function of pressure. The inset shows zoomed area “A” where two trends T1 and T2 represent pressure induced progressive feature peak position drifting and feature peak intensity decrease, respectively.